

Article

CTAB Enhanced Room-Temperature Detection of NO₂ Based on MoS₂-Reduced Graphene Oxide Nanohybrid

Wenbo Li ^{1,2,3}, Hao Li ^{1,2,3}, Rong Qian ^{1,3,*} , Shangjun Zhuo ^{1,3}, Pengfei Ju ^{4,*} and Qiao Chen ⁵

¹ National Center for Inorganic Mass Spectrometry in Shanghai, Shanghai Institute of Ceramics, Chinese Academy of Sciences, Shanghai 200050, China; hymnek@hotmail.com (W.L.); lh960714211@163.com (H.L.); sjzhuo@mail.sic.ac.cn (S.Z.)

² School of Material Science and Engineering, University of Shanghai for Science and Technology, Shanghai 200093, China

³ Center of Materials Science and Optoelectronics Engineering, University of Chinese Academy of Sciences, Beijing 100049, China

⁴ Shanghai Aerospace Equipment Manufacturer, Shanghai 200245, China

⁵ Department of Chemistry, School of Life Sciences, University of Sussex, Brighton BN1 9QJ, UK; qiao.chen@sussex.ac.uk

* Correspondence: qianrong@mail.sic.ac.cn (R.Q.); jupengfei10@163.com (P.J.)

Abstract: A new NO₂ nanohybrid of a gas sensor (CTAB-MoS₂/rGO) was constructed for sensitive room-temperature detection of NO₂ by 3D molybdenum disulfide (MoS₂) and reduced graphene oxide (rGO), assisted with hexadecyl trimethyl ammonium bromide (CTAB). In comparison with MoS₂ and MoS₂/rGO, the BET and SEM characterization results depicted the three-dimensional structure of the CTAB-MoS₂/rGO nanohybrid, which possessed a larger specific surface area to provide more active reaction sites to boost its gas-sensing performance. Observations of the gas-sensing properties indicated that the CTAB-MoS₂/rGO sensor performed a high response of 45.5% for 17.5 ppm NO₂, a remarkable selectivity of NO₂, an ultra-low detection limit of 26.55 ppb and long-term stability for a 30-day measurement. In addition, the response obtained for the CTAB-MoS₂/rGO sensor was about two to four times that obtained for the MoS₂/rGO sensor and the MoS₂ sensor toward 8 ppm NO₂, which correlated with the heterojunction between MoS₂ and rGO, and the improvement in surface area and conductivity correlated with the introduction of CTAB and rGO. The excellent performance of the CTAB-MoS₂/rGO sensor further suggested the advantage of CTAB in assisting a reliable detection of trace NO₂ and an alternative method for highly efficiently detecting NO₂ in the environment.

Keywords: hexadecyl trimethyl ammonium bromide (CTAB); reduced graphene oxide (rGO); nanohybrid; NO₂ gas-sensing properties; room temperature



Citation: Li, W.; Li, H.; Qian, R.; Zhuo, S.; Ju, P.; Chen, Q. CTAB Enhanced Room-Temperature Detection of NO₂ Based on MoS₂-Reduced Graphene Oxide Nanohybrid. *Nanomaterials* **2022**, *12*, 1300. <https://doi.org/10.3390/nano12081300>

Academic Editors: Filippo Giannazzo and Ivan Shteplyuk

Received: 5 March 2022

Accepted: 7 April 2022

Published: 11 April 2022

Publisher's Note: MDPI stays neutral with regard to jurisdictional claims in published maps and institutional affiliations.



Copyright: © 2022 by the authors. Licensee MDPI, Basel, Switzerland. This article is an open access article distributed under the terms and conditions of the Creative Commons Attribution (CC BY) license (<https://creativecommons.org/licenses/by/4.0/>).

1. Introduction

Although nitrogen dioxide (NO₂) matters a lot in the industrial, farming and health-care fields, it is also one kind of poisonous gas—harmful to environment and human health. In general, NO₂ is generated from burning fossil fuels or automotive emissions, leading to a lot of serious diseases such as pulmonary, cardiovascular and cardiac diseases, even at low concentrations [1,2]. On this account, many analytical techniques have been applied for monitoring and detecting NO₂, including electrochemical, optical, chemiresistive, spectroscopies methods and so on [3]. However, these techniques usually require time-consuming sample treatment procedures, expensive and bulky instruments that could not provide convenient and real-time online detection for the leaking, diffusing or transferring of NO₂ gas [4,5]. Because of many superiorities, including low cost, easy operation and rapid, real-time detection and warning, portable semiconductor chemiresistive gas sensors can offer an alternative method for the effective monitoring and detecting of NO₂ [6]. Nowadays,

portable semiconductor chemiresistive gas sensors have been extensively applied for smart environmental monitoring and have shown a higher commercial application potential [7].

For the abundant vacancies and oxygen-containing functional groups on composite materials containing [8] graphene and derivatives, the sensors have been utilized for practical applications and have attracted considerable attention for detecting poisonous gas in environmental and industrial fields and monitoring exhaled air. Nowadays, rGO sensors have become one of the most common gas sensors. Wang et al. reported a novel NO₂ sensor produced with the heterostructure of ZnO-SnO₂ on rGO, which displayed a high response of 141.0% toward 5 ppm of NO₂ at room temperature [9]. Liu et al. synthesized a NO₂ sensor by ZnO-rGO hybrids, whose response towards 5 ppm NO₂ operating at room temperature was 25.6%. The response time and recovery time towards 5 ppm were 165 s and 499 s, respectively [10]. Chan et al. prepared rGO-In₂O₃ hybrid nanostructure sensors, which presented a fine response of 22.3% toward 500 ppb NO₂ at 150 °C [11]. Meanwhile, the two-dimensional layered nano-material of MoS₂ also drew much attention on account of its prominent semiconductor properties and high surface-to-volume ratio [12]. Yang et al. described the main attributes of two-dimensional nanomaterials and demonstrated that an intense interaction existed between MoS₂ and NO₂ molecules, suggesting that MoS₂ could be one special material for sensitively detecting NO₂ [13,14]. To a certain extent, MoS₂-based gas sensors exhibited better sensing properties than some carbon materials such as graphene and CNT [15]. However, MoS₂-based gas sensors are still facing numerous challenges, such as short lifetime, tardy response or recovery rate, poor gas selectivity and complicated fabrication, which might limit their development or application [16–20].

Surfactants are known for their capability for controlling crystal morphology in the fabrication of inorganic nanomaterials [21]. CTAB is a common surfactant, and it is used extensively for synthesizing nanoparticles [22]. Zhang et al. synthesized a three-dimensional MoS₂ nanoflower with a size of around 300 nm in the presence of CTAB, and the MoS₂-based sensor displayed a response of 60% to 50 ppm NO₂ at 100 °C, but it suffered a low response of almost 8% at room temperature [23]. Lin et al. reported MoS₂/rGO composites synthesized with CTAB, which had a larger surface area than those synthesized using TritonX-100 or sodium dodecyl sulfonate [24]. Notably, the strategy of employing a surfactant for nanocomposite fabrication could improve gas adsorption on the material's surface and promote gas-sensing performance.

In our work, a new CTAB-MoS₂/rGO nanohybrid sensor was fabricated for room temperature, detecting NO₂ based on hydrothermal and ultrasonic processes. Under ambient conditions, the gas-sensing performances of the CTAB-MoS₂/rGO, MoS₂ and MoS₂/rGO sensors were systematically studied, showing that the response obtained for the CTAB-MoS₂/rGO sensor was about four times that obtained for the MoS₂ sensor and two times that obtained for the MoS₂/rGO sensor to 8 ppm NO₂. Under ambient conditions, the CTAB-MoS₂/rGO sensor performed a high response of 45.5% for 17.5 ppm NO₂, an ultralow detection limit of 26.55 ppb, excellent selectivity for NO₂ and long-term stability for a 30-day persistent property test. The remarkable gas-sensing performance possibly owed to the formation of a heterojunction between the MoS₂ and rGO, the increase in the number of active sites with the introduction of CTAB and the improvement of conductivity with rGO.

2. Materials and Methods

2.1. Materials and Chemicals

The reduced graphene oxide (rGO) dispersion was received from Chengdu Organic Chemicals Co. Ltd. (Chengdu, China) Thiourea (N₂H₄CS, 99%) and hexadecyl trimethyl ammonium bromide (CTAB, 99%) were obtained from Shanghai Macklin Biochemical Co. Ltd. (Shanghai, China). The sodium molybdate dihydrate (Na₂MoO₄·2H₂O, 99%) was purchased from Shanghai Adamas-beta Co. Ltd. (Shanghai, China).

2.2. Sample Preparation

For the CTAB-MoS₂ nanohybrid synthesis, in a typical run, 2 mmol NaMoO₄·2H₂O and 10 mmol thiourea were fully dispersed into 70 mL deionized water, then followed by sonication for 30 min. Subsequently, 210 mg CTAB was dissolved into the above solution through extra sonication for 30 min (the details about optimization and the XRD graph are in Figure S1). Next, the solution was poured into a 100 mL autoclave and kept at 210 °C for 24 h. The CTAB-MoS₂ powder was obtained after centrifugation and washed with deionized water and anhydrous ethanol. The MoS₂ was prepared with the same procedure without the CTAB. In the CTAB-MoS₂/rGO fabrication process, 10 mg of the obtained CTAB-MoS₂ powder was added into 1 mL ethanol, followed by sonication for 30 min in order to completely disperse. After completely dispersing, 0.1 mL of the rGO dispersion was dropped into the above solution under sonication for 1 h to synthesize the CTAB-MoS₂/rGO hybrid. The MoS₂/rGO composite was also synthesized with the same procedure. A diagram of the preparation of the composite is illustrated in Figure 1.

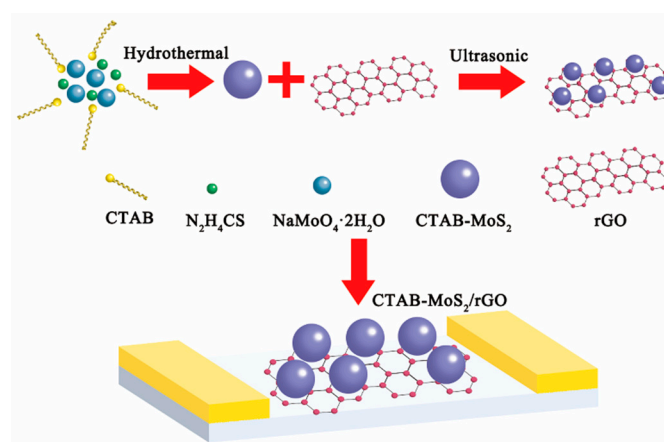


Figure 1. The preparation of CTAB-MoS₂/rGO nanohybrid.

2.3. Characterization of Materials

The morphologies of the sensing materials were analyzed by a scanning electron microscope (SEM, SU8220, Hitachi, Tokyo, Japan) and a transmission electron microscope (TEM, JEM-2100F, JEOL). Crystallinity information was obtained by X-ray diffraction (XRD, D8 ADVANCE, Bruker, Cu α , 380 eV). The composition information was characterized by X-ray photoelectron spectroscopy (XPS, ESCALAB 250, Al X-ray source, 0.5 eV). A confocal Raman microscope (in Via RENISHAW) was utilized to obtain Raman spectra.

2.4. Fabrication of CTAB-MoS₂/rGO Sensor

The CTAB-MoS₂/rGO sensor was fabricated on interdigital electrodes, which were composed of CTAB-MoS₂/rGO sensing materials and interdigital electrodes. The interdigital electrodes were cleaned under sonication with acetone, deionized water and ethanol, respectively, before use. The composite suspension was obtained by adding 10 mg hybrid powder into 1 mL ethanol under sonication for 0.5 h. After that, 0.5 μ L of the solution was dropped onto the cleaned interdigital electrodes by pipette. Then, the interdigital electrodes were kept in a 60 °C oven for 3 h to remove the extra ethanol.

2.5. Measurement of Gas-Sensing Properties

In order to observe the gas-sensing properties, homemade gas-sensing test equipment was constructed and demonstrated, which consisted of gas cylinders, a gas-sensing chamber, a plastic conduit and a resistance acquisition device (see Figure S2 for fabrication details). The gas cylinders were filled with dry air and dry NO₂, respectively. The gas-sensing chamber contained a 300 mL cylindrical cavity with several holes for gas injection and venting. The resistance of the sensors was obtained with a Keithley 2701 resistance

acquisition device. The bubbling method was used to adjust the moisture of injected gas. Typically, dry air was passed through a cylindrical cavity with a certain volume of water to obtain a relative humidity (RH), and then mixed with dry NO₂ [25,26]. Various concentrations of NO₂ were gained by mixing the wet air with dry NO₂, and all the gas flow ratios were regulated by mass flow controllers (MFC). The final flow rate of gas was fixed as 400 mL/min. The response value of the sensor was determined by $(\Delta R)/R_0 \times 100\%$, where $\Delta R = (R_0 - R_g)$, R_0 was the resistance value in the air and R_g was the resistance value in NO₂. For all the gas-sensing performance measurements, NO₂ was introduced into the gas-sensing chamber for 10 min. The following sensing tests were implemented at room temperature and 58% RH, if without any special indication.

3. Results

3.1. Morphological and Structural Characterization

Figure 2a suggests that the crystal planes of pure MoS₂ were assigned to the (002), (004), (101), (103), (006), (105) and (110) of the hexagonal phase. It has been proven that 2H-MoS₂ had better semiconductor properties and more thermal stability than 1T-MoS₂ and 3R-MoS₂ [27]. The (002) crystal plane indicated stacking a layered structure along the c-axis in bulk MoS₂ [28]. When the rGO and CTAB were introduced to the hybrid, the main peaks of the (004), (101), (103), (006), (105) and (110) crystal planes became weaker or even disappeared, to restrain the aggregation and restacking of the layered structure of the MoS₂ [29]. Meanwhile, no peak around 2 theta of 25 degrees appeared for the MoS₂/rGO and CTAB-MoS₂/rGO composites, which could suggest a decrease in the layer stacking of the rGO with the existence of MoS₂. The XRD investigations demonstrated the prepared MoS₂ was in accordance with JCPDS card 37-1492, and some peaks of the MoS₂ became weaker or disappeared, which was beneficial for the promotion of sensing performance [30].

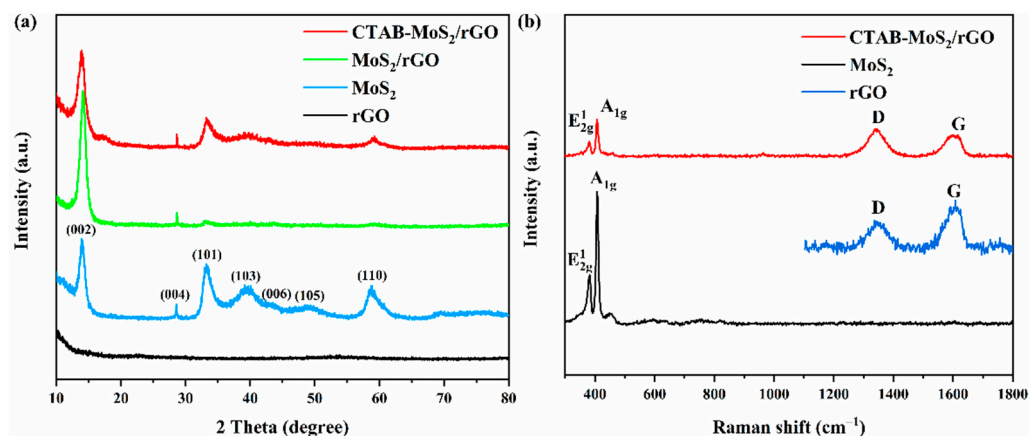


Figure 2. (a) XRD characterization of rGO, MoS₂, MoS₂/rGO and CTAB-MoS₂/rGO; (b) Raman characterization of rGO, MoS₂ and CTAB-MoS₂/rGO.

The structure of the CTAB-MoS₂/rGO was carefully studied by Raman characterization. Figure 2b shows that two typical peaks at 380.9 cm⁻¹ and 407.5 cm⁻¹ were regarded as the in-plane vibration E_{2g}¹ and the out-of-plane vibration A_{1g}¹ of the MoS₂. The peak position of E_{2g}¹ and A_{1g}¹ could be applied to calculate the layer numbers of the MoS₂ [31]. The Raman shift difference was 26.6 cm⁻¹, which could suggest that the MoS₂ had a multi-layer structure. Meanwhile, Figure 2b also depicts a D band (1348.39 cm⁻¹) and a G band (1593.39 cm⁻¹) of rGO, which indicated that the hybrid of MoS₂/rGO was successfully formed by the introduction of rGO. In addition, the D band was induced by defects, and the G band was attributed to sp² hybridized carbon atoms [32].

The microstructures and morphologies of the sensing materials were further characterized through SEM. Figure 3a shows a three-dimensional flower-like structure of the MoS₂ with multiple nanosheets. The thin nanosheets can be distinctly observed in Figure 3b. Figure 3c suggests that the rGO was closely attached to the MoS₂ micro-flower for the formation of the MoS₂/rGO hybrids, which was consistent with the investigation of Raman spectra. The image of the CTAB-MoS₂/rGO is presented in Figure 3d, and the elemental mapping results are presented in Figure 3e–h. It was clear that the CTAB-MoS₂/rGO material mainly contained C, O, Mo and S with homogeneous distribution. Furthermore, the TEM images in Figure 3i–l present the morphologies of the rGO, MoS₂, MoS₂/rGO and the CTAB-MoS₂/rGO, respectively. The high-magnification TEM image further demonstrates that the molybdenum disulfide was multi-layered.

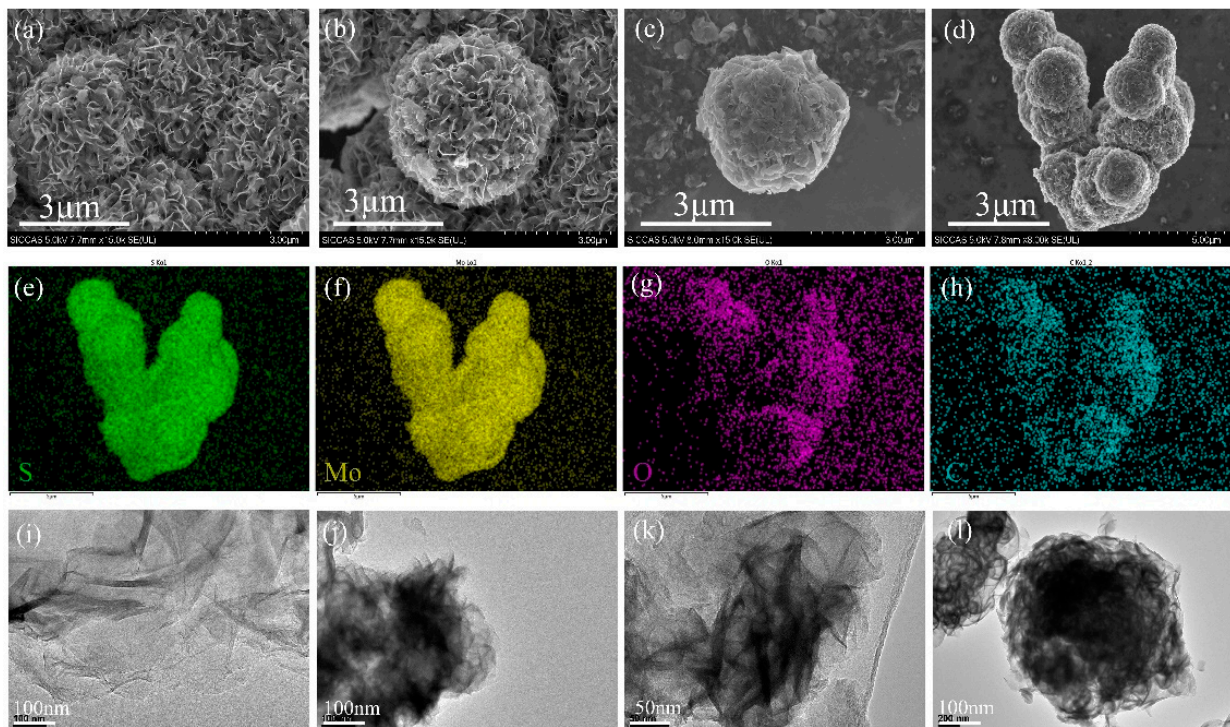


Figure 3. (a,b) SEM images of MoS₂. (c,d) SEM images of MoS₂/rGO and CTAB-MoS₂/rGO. (e–h) The elemental mapping of CTAB-MoS₂/rGO. TEM images of (i) rGO, (j) MoS₂, (k) MoS₂/rGO, (l) CTAB-MoS₂/rGO.

Figure 4a indicates the survey spectrum, suggesting the presence of C, Mo, S and O elements. Figure 4b demonstrates that the typical peaks at 284.6 and 286.6 eV could be assigned to C-C of the graphene skeleton and C-O bond [33]. Figure 4c suggests two valence states for Mo peaks. The peak at 232.2 eV could be assigned to Mo⁴⁺ 3d_{3/2}, and the peak at 229.1 eV was assigned to Mo⁴⁺ 3d_{5/2} [34]. The small peak at 235.4 eV could have resulted from Mo⁶⁺ 3d_{3/2}, which was potentially ascribed to the low amount of MoO₃ in the composite as reported in the previous literature [35]. The peak at 226.3 eV could be assigned to S 2s. Moreover, Figure 4d suggests that the peaks of 163.0 eV and 161.9 eV could be assigned to S²⁻ 2p_{1/2} and S²⁻ 2p_{3/2} of the MoS₂ [36].

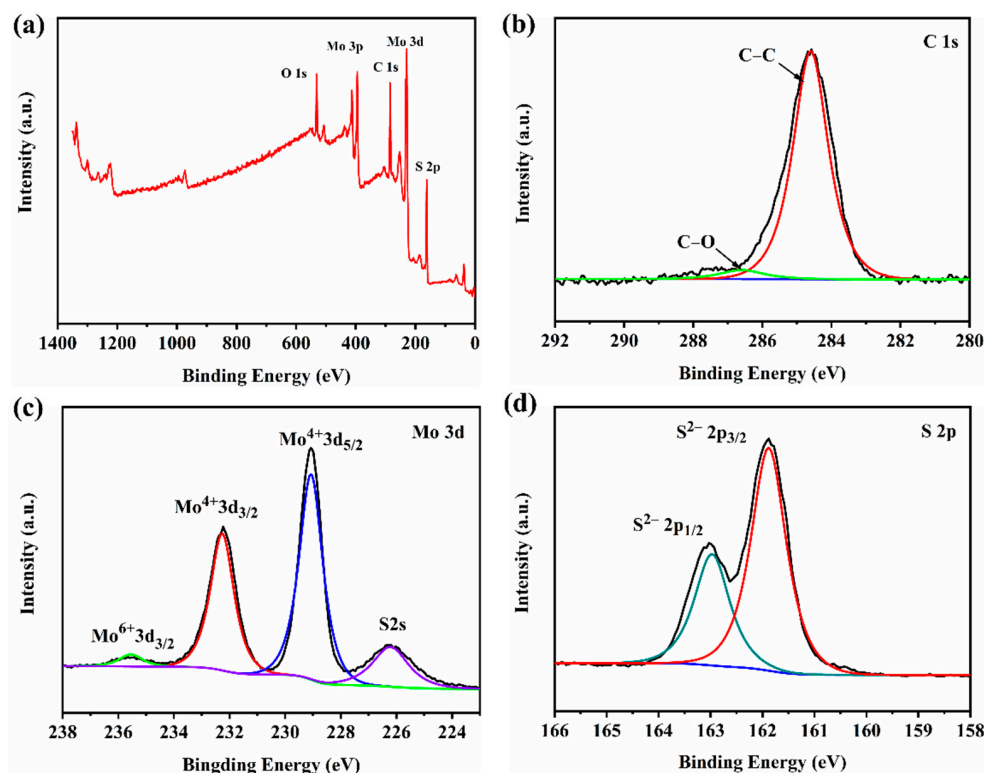


Figure 4. XPS spectra of CTAB-MoS₂/rGO: (a) survey spectrum, (b) C 1s, (c) Mo 3d and (d) S 2p.

3.2. Gas-Sensing Properties

The sequential dynamic reversible performance of the CTAB-MoS₂/rGO sensor was investigated by exposing the CTAB-MoS₂/rGO sensor toward various concentrations of NO₂ of 1–17.5 ppm. The response values were 45.52%, 37.64%, 35.50%, 31.75%, 24.19% and 14.45% for 17.5 ppm, 8 ppm, 6 ppm, 4 ppm, 2 ppm and 1 ppm of NO₂, respectively, which suggests that the CTAB-MoS₂/rGO sensor could monitor NO₂ in a wide concentration range sensitively. To further study the sensor's properties, a linear fitting curve was plotted for the CTAB-MoS₂/rGO sensor's response values versus lg (NO₂ concentration). Figure 5b suggests that the response values had an excellent linear relationship with lg (NO₂ concentration), and its correlation coefficient (R^2) was 0.991, which could demonstrate the reliable responses toward 1–17.5 ppm NO₂. The detection limit in this work could be calculated by a formula [37]. By calculation, the LOD was 26.55 ppb, which was lower than the limit of 53 ppb claimed by the U.S. Environmental Protection Agency [38] (see Figure S3 for the calculation of the detection limit).

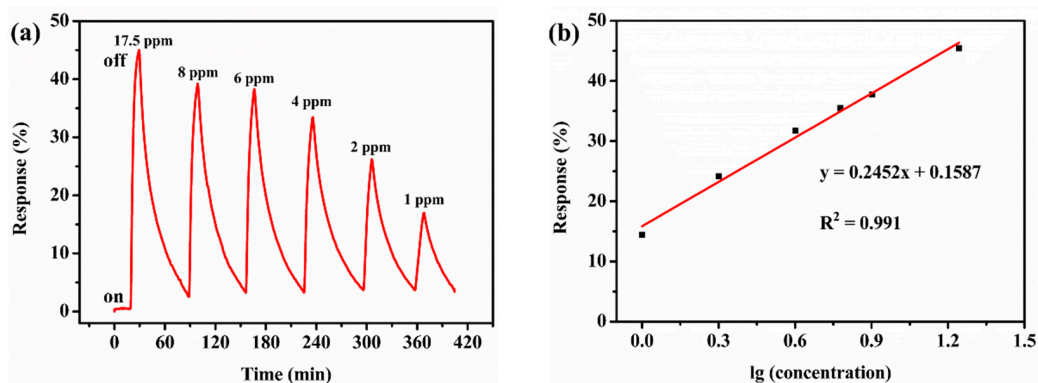


Figure 5. (a) Gas-sensing properties sensitivity of the CTAB-MoS₂/rGO toward NO₂ with concentration of 1–17.5 ppm at room temperature, RH of 58%. (b) The linear fitting curve between NO₂ concentration and response for CTAB-MoS₂/rGO.

Subsequently, the comparisons of the response and recovery properties were tested at room temperature and 58% RH for the CTAB-MoS₂/rGO, MoS₂/rGO and MoS₂ sensors toward 8 ppm NO₂. The MoS₂ sensor performed a response of 9.7%. The MoS₂/rGO sensor performed a response of 21.35%, which was two times that of the MoS₂ sensor. The increased response demonstrated that the addition of rGO mattered a lot for improving the sensing properties, owing to the generation of a heterojunction between the MoS₂ and rGO and the excellent performance of the rGO. More importantly, the CTAB-MoS₂/rGO sensor displayed a response of 37.64% toward 8 ppm NO₂, which was nearly two times the response for the MoS₂/rGO sensor and four times the response for the pure MoS₂ sensor. Moreover, the gradually increased specific surface area (Figure 6b) for the MoS₂, MoS₂/rGO and CTAB-MoS₂/rGO might facilitate the distinct promotion of the gas-sensing properties.

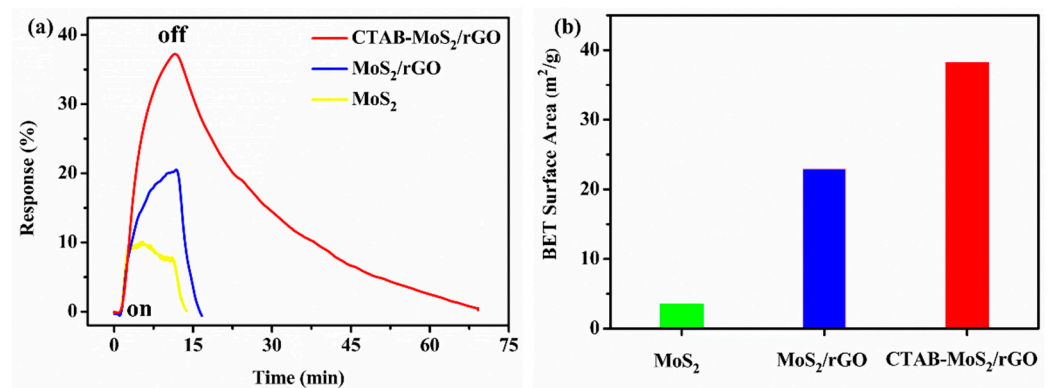


Figure 6. (a) The comparisons of the response and recovery properties of MoS₂, MoS₂/rGO and CTAB-MoS₂/rGO sensors toward 8 ppm NO₂ at room temperature and (b) the BET surface area of sensing materials.

Long-term stability was studied through continuously measuring the response values of the CTAB-MoS₂/rGO sensor toward 8 ppm NO₂ for four weeks (Figure 7a). The results showed that the response values decreased only 5.81% from 37.64% of the first week to 31.83% of the fourth week, and always maintained a high response to NO₂ during the four weeks. The results indicated the gas sensor was capable of detecting NO₂ with a remarkable repeatability and superior long-term stability.

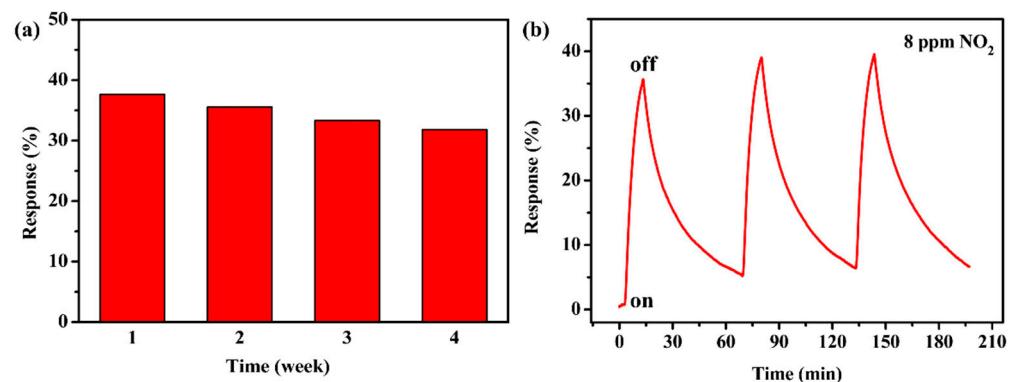


Figure 7. (a) Long-term stability of CTAB-MoS₂/rGO sensor toward 8 ppm NO₂ for four weeks and (b) repeatability of the CTAB-MoS₂/rGO sensor.

The repeatability was tested by exposing the CTAB-MoS₂/rGO sensor to 8 ppm NO₂ for three response–recovery cycles at room temperature and 58% RH (Figure 7b). It was noticeable that the response values maintained practically the same values after three cycles without an obvious response drop, which could confirm splendid repeatability for the CTAB-MoS₂/rGO sensor.

Since selectivity is a crucial property for gas sensors in real environments, the selectivity of the CTAB-MoS₂/rGO sensor was measured by exposing it to 17.5 ppm of NO₂, 100 ppm of NH₃, 1000 ppm of methanol, ethanol, isopropanol and acetone. Figure 8a shows that the response value toward 17.5 ppm NO₂ was far higher than the higher concentration of all of the interfering gas species, suggesting an outstanding selectivity of the CTAB-MoS₂/rGO sensor toward NO₂. The extremely low response to high concentrations of methanol, ethanol, isopropanol and acetone may have resulted from the high activation energy barrier of the reaction between the sensing material surface and VOCs [39].

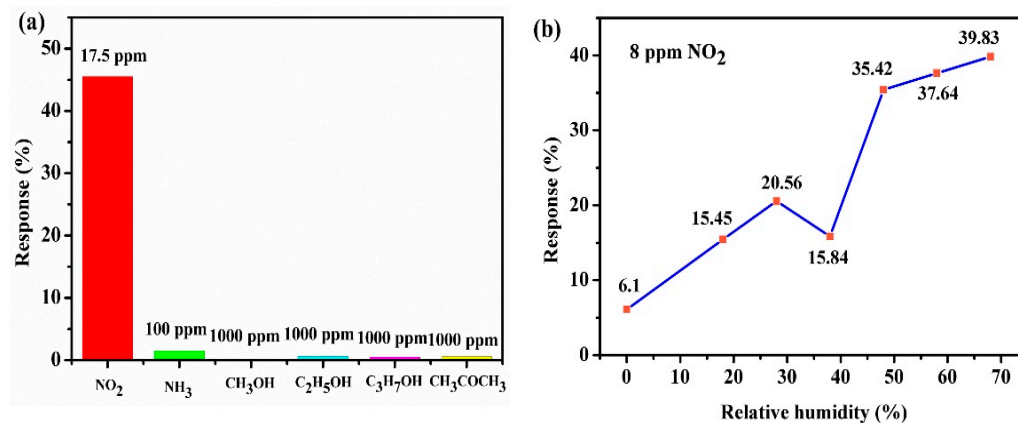


Figure 8. (a) Selectivity of CTAB-MoS₂/rGO sensor toward various gases, and (b) humidity influence on response for CTAB-MoS₂/rGO sensor toward 8 ppm NO₂.

The influence of RH on gas-sensing properties was further explored by exposing the CTAB-MoS₂/rGO sensor toward 8 ppm NO₂ at different moisture levels (0–68% RH), and the result is shown in Figure 8b. Here, RH in the gas-sensing chamber was controlled by letting dry air pass through a cylindrical cavity of water and mixing it with dry NO₂. Before injecting NO₂ into the gas-sensing chamber, the CTAB-MoS₂/rGO sensor was exposed to wet air with a desired relative humidity. After the resistance was relatively stable, 8 ppm NO₂ was introduced to the gas chamber. The sensor response (6.1%) was very low when exposed to 8 ppm of dry NO₂. As the relative humidity rose from 0 to 28%, the response rose from 6.1% to 20.56% accordingly. While increasing the moisture level to 38% RH, the response decreased to 15.84%, which could be due to the reduction in the number of active reaction sites. Since the gas adsorption sites on the MoS₂/rGO were occupied by abundant water, the number of active reaction sites and the sensitivity decreased. The response increased dramatically as the relative humidity continued to increase to a higher moisture level (38–68% RH). It is possible that the electrons of CTAB-MoS₂/rGO were captured by NO₂ due to its higher electrophilic property to form NO₂[−], and NO₂[−] simultaneously reacted with the adsorbed oxygen ion to form NO₃[−]. NO₃[−] was dominant even though NO₂[−] and NO₃[−] could exist at the same time when the moisture level increased to a high relative humidity. The binding energy of NO₃[−] was higher than NO₂[−], which could result in the enhancement of the response value at a higher moisture level [40]. However, when the relative humidity was at 48–68%, the response values were almost similar, which was possibly caused by the saturation of the impact of the relative humidity on response. The results indicated that the sensors showed excellent gas-sensing properties in high-RH ambient, qualifying them for detecting NO₂ gas in a high-RH environment. In addition, the CTAB-MoS₂/rGO sensor showed excellent sensitivity and a low detection limit at room temperature compared to the previous TMDs-based sensors and rGO-based sensors (Table 1).

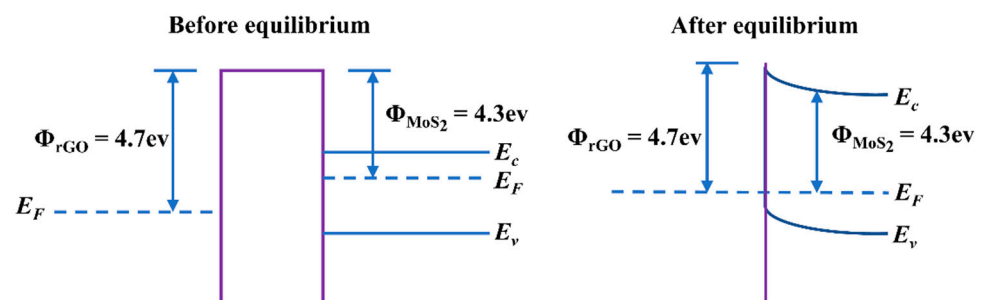
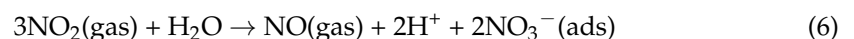
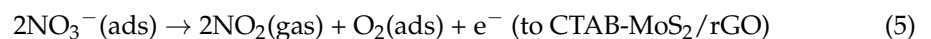
Table 1. Comparison of previously reported TMDs-based sensors, rGO-based sensors and CTAB-MoS₂/rGO sensor.

Materials	Temperature (°C)	Concentration (ppm)	Response	LOD (ppb)	References
MoS ₂ /CNT	RT	25	5% ^a	25	[41]
ZnO-rGO	RT	5	25.6% ^a		[9]
NbS ₂	RT	5	18% ^a	241.02	[42]
MoS ₂ /SnO ₂	RT	5	5% ^a	500	[43]
MoS ₂ /rGO	RT	5	14.28% ^a	50	[32]
rGO/Co ₃ O ₄	RT	5	26.8% ^a	50	[44]
SnS ₂ /rGO	RT	8	49.8% ^b	8.7	[45]
rGO/ZnO	RT	15	45% ^a		[46]
MoS ₂ /ZnO	RT	5	3050% ^c	50	[47]
In ₂ O ₃ /MoS ₂	RT	10	50 ^d	8.8	[48]
CTAB-MoS ₂ /rGO	RT	8	37.64% ^a	26.55	Our work

^a $(R_0 - R_g)/R_0$; ^b $\Delta G/G_0$; ^c $(I_g - I_0)/I_0$; ^d R_g/R_0 . RT = room temperature.

4. Discussion

According to previous reports [49], the active species NO₃⁻ originated from NO₂ may play a significant role in causing the resistance changes of sensing materials. Based on the theory and the experiments [50], a possible mechanism was proposed and illustrated for the CTAB-MoS₂/rGO sensor (Figure 9). When the CTAB-MoS₂/rGO sensor was exposed to the air, the oxygen molecules in the air would adsorb electrons in the gas-sensitive material to form chemically adsorption oxygen O₂⁻. When the CTAB-MoS₂/rGO hybrid contacted NO₂ gas, the electrons would transfer from the hybrid to NO₂ to form NO₂⁻, resulting in the rise of hole concentration and the decline of resistance. Meanwhile, NO₂ with strong electron absorption ability could also seize electrons from the material and react with the previous O₂⁻ to generate NO₃⁻. While the sensor was exposed to air again, NO₃⁻ would desorb from the sensing material surface, and the electron would return to the hybrid, thus the resistance would recover to the initial state. Moreover, the formation of the heterojunction between the MoS₂ and rGO shows that electrons are transported from the conduction band of MoS₂ to that of rGO [51]. The increase in the specific surface area with CTAB and the improvement of conductivity with rGO might result in the enhancement of the gas-sensing properties of the CTAB-MoS₂/rGO sensor. The whole reaction is as follows:

**Figure 9.** The diagram of energy band at CTAB-MoS₂/rGO interfaces.

5. Conclusions

In the present work, an efficient CTAB-MoS₂/rGO gas sensor was successfully prepared for room-temperature detection of NO₂ with the assistance of surfactant CTAB. The sensing properties of the MoS₂, MoS₂/rGO and CTAB-MoS₂/rGO sensors were systematically investigated by exposure to NO₂. The introduction of rGO and surfactant CTAB could significantly promote sensitivity to NO₂, and the capability of recovery was slightly decreased due to the effect of rGO. The investigations demonstrated that the CTAB-MoS₂/rGO sensor manifested an excellent response, remarkable repeatability, long-term stability and selectivity toward NO₂. The great sensing performance could result from the generation of a heterojunction, the positive effect of CTAB and the good conductivity of rGO. The investigations also suggested that the surfactant was a great prospect for fabricating high properties of room-temperature gas sensors. Further research in this area is being implemented in our laboratory.

Supplementary Materials: The following are available online at <https://www.mdpi.com/article/10.3390/nano12081300/s1>, Figure S1. XRD of different concentrations of CTAB-MoS₂, Figure S2. SEM images of CTAB-MoS₂; (a) 0 mg/mL (b) 1.5 mg/mL (c) 3 mg/mL (d) 6 mg/mL, Figure S3. Schematic image of the gas sensor measurement system, Table S1. A fifth order polynomial fitting result.

Author Contributions: Conceptualization, W.L., H.L. and R.Q.; investigation, W.L., S.Z. and P.J.; supervision, R.Q. and Q.C.; writing—original draft preparation, W.L. and H.L.; writing—review and editing, S.Z., R.Q., P.J. and Q.C. All authors have read and agreed to the published version of the manuscript.

Funding: This research was funded by Shanghai Science and Technology Innovation Action Project (Grant No. 20142201100), Shanghai Intergovernmental International Cooperation Project (Grant No. 19520712000) and Shanghai Technical Platform of Testing on Inorganic Materials (Grant No. 19DZ2290700).

Institutional Review Board Statement: This study did not involve humans or animals.

Informed Consent Statement: Informed consent was obtained from all subjects involved in the study.

Data Availability Statement: The data presented in this study are available on request from the corresponding author.

Conflicts of Interest: The authors declare no conflict of interest.

References

1. Rani, S.; Kumar, M.; Singh, Y.; Tomar, M.; Sharma, A.; Gupta, V.; Singh, V.N. NO₂ Gas Sensor Based on SnSe/SnSe₂ pn Hetrojunction. *J. Nanosci. Nanotechnol.* **2021**, *21*, 4779–4785. [[CrossRef](#)] [[PubMed](#)]
2. Zhao, S.; Shen, Y.; Maboudian, R.; Carraro, C.; Han, C.; Liu, W.; Wei, D. Facile synthesis of ZnO-SnO₂ hetero-structured nanowires for high-performance NO₂ sensing application. *Sens. Actuators B* **2021**, *333*, 129613. [[CrossRef](#)]
3. Zhu, Z.; Lin, S.J.; Wu, C.H.; Wu, R.J. Synthesis of TiO₂ nanowires for rapid NO₂ detection. *Sens. Actuators A* **2018**, *272*, 288–294. [[CrossRef](#)]
4. Wang, X.D.; Wolfbeis, O.S. Fiber-optic chemical sensors and biosensors (2013–2015). *Anal. Chem.* **2016**, *88*, 203–227. [[CrossRef](#)]
5. Chang, S.C.; Stetter, J.R. Electrochemical NO₂ gas sensors: Model and mechanism for the electroreduction of NO₂. *Electroanalysis* **1990**, *2*, 359–365. [[CrossRef](#)]
6. Yang, B.; Myung, N.V.; Tran, T.T. 1D metal oxide semiconductor materials for chemiresistive gas sensors: A review. *Adv. Electron. Mater.* **2021**, *7*, 2100271. [[CrossRef](#)]
7. Nasiri, N.; Clarke, C. Nanostructured chemiresistive gas sensors for medical applications. *Sensors* **2019**, *19*, 462. [[CrossRef](#)]
8. Meng, F.L.; Guo, Z.; Huang, X.J. Graphene-based hybrids for chemiresistive gas sensors. *TrAC Trends Anal. Chem.* **2015**, *68*, 37–47. [[CrossRef](#)]
9. Wang, Z.; Gao, S.; Fei, T.; Liu, S.; Zhang, T. Construction of ZnO/SnO₂ heterostructure on reduced graphene oxide for enhanced nitrogen dioxide sensitive performances at room temperature. *ACS Sens.* **2019**, *4*, 2048–2057. [[CrossRef](#)]
10. Liu, S.; Yu, B.; Zhang, H.; Fei, T.; Zhang, T. Enhancing NO₂ gas sensing performances at room temperature based on reduced graphene oxide-ZnO nanoparticles hybrids. *Sens. Actuators B* **2014**, *202*, 272–278. [[CrossRef](#)]
11. Na, C.W.; Kim, J.H.; Kim, H.J.; Woo, H.S.; Gupta, A.; Kim, H.K.; Lee, J.H. Highly selective and sensitive detection of NO₂ using rGO-In₂O₃ structure on flexible substrate at low temperature. *Sens. Actuators B* **2018**, *255*, 1671–1679.

12. Wan, P.; Yang, W.; Wang, X.; Hu, J.; Zhang, H. Reduced graphene oxide modified with hierarchical flower-like $\text{In}(\text{OH})_3$ for NO_2 room-temperature sensing. *Sens. Actuators B* **2015**, *214*, 36–42. [[CrossRef](#)]
13. Yang, W.; Gan, L.; Li, H.; Zhai, T. Two-dimensional layered nanomaterials for gas-sensing applications. *Inorg. Chem. Front.* **2016**, *3*, 433–451.
14. Late, D.J.; Huang, Y.K.; Liu, B.; Acharya, J.; Shirodkar, S.N.; Luo, J.; Yan, A.; Charles, D.; Waghmare, U.V.; Dravid, V.P.; et al. Sensing behavior of atomically thin-layered MoS_2 transistors. *ACS Nano* **2013**, *7*, 4879–4891. [[PubMed](#)]
15. Perkins, F.K.; Friedman, A.L.; Cobas, E.; Campbell, P.M.; Jernigan, G.G.; Jonker, B.T. Chemical vapor sensing with monolayer MoS_2 . *Nano Lett.* **2013**, *13*, 668–673. [[CrossRef](#)]
16. Kumar, R.; Goel, N.; Kumar, M. UV-activated MoS_2 based fast and reversible NO_2 sensor at room temperature. *ACS Sens.* **2017**, *2*, 1744–1752. [[CrossRef](#)]
17. Wang, S.; Chen, W.; Li, J.; Song, Z.; Zhang, H.; Zeng, W. Low working temperature of ZnO-MoS_2 nanocomposites for delaying aging with good acetylene gas-sensing properties. *Nanomaterials* **2020**, *10*, 1902. [[CrossRef](#)]
18. Lim, N.; Lee, J.S.; Byun, Y.T. Negatively-doped single-walled carbon nanotubes decorated with carbon dots for highly selective NO_2 detection. *Nanomaterials* **2020**, *10*, 2509. [[CrossRef](#)]
19. Zeng, Y.; Lin, S.; Gu, D.; Li, X. Two-dimensional nanomaterials for gas sensing applications: The role of theoretical calculations. *Nanomaterials* **2018**, *8*, 851. [[CrossRef](#)]
20. Seo, W.S.; Kim, D.K.; Han, J.H.; Park, K.B.; Ryu, S.C.; Min, N.K.; Kim, J.H. Functionalization of Molybdenum Disulfide via Plasma Treatment and 3-Mercaptopropionic Acid for Gas Sensors. *Nanomaterials* **2020**, *10*, 1860. [[CrossRef](#)]
21. Zhao, Z.; Bai, Y.; Ning, W.; Fan, J.; Gu, Z.; Chang, H.; Yin, S. Effect of surfactants on the performance of 3D morphology $\text{W}_{18}\text{O}_{49}$ by solvothermal synthesis. *Appl. Surf. Sci.* **2019**, *471*, 537–544. [[CrossRef](#)]
22. Nagyné-Kovács, T.; Studnicka, L.; Lukács, I.E.; László, K.; Pasierb, P.; Szilágyi, I.M.; Pokol, G. Hydrothermal synthesis and gas sensing of monoclinic MoO_3 nanosheets. *Nanomaterials* **2020**, *10*, 891. [[CrossRef](#)] [[PubMed](#)]
23. Zhang, Y.; Zeng, W.; Li, Y. Hydrothermal synthesis and controlled growth of hierarchical 3D flower-like MoS_2 nanospheres assisted with CTAB and their NO_2 gas sensing properties. *Appl. Surf. Sci.* **2018**, *455*, 276–282. [[CrossRef](#)]
24. Hongtao, L.; Zichen, X.; Lina, Z.; Zhiqiang, Z.; Li, X. The effects of different surfactants on the morphologies and electrochemical properties of MoS_2 /reduced graphene oxide composites. *Chem. Phys. Lett.* **2019**, *716*, 6–10. [[CrossRef](#)]
25. Wu, J.; Sun, Y.M.; Wu, Z.; Li, X.; Wang, N.; Tao, K.; Wang, G.P. Carbon nanocoil-based fast-response and flexible humidity sensor for multifunctional applications. *ACS Appl. Mater. Interfaces* **2019**, *11*, 4242–4251. [[CrossRef](#)]
26. Wu, J.; Wu, Z.; Tao, K.; Liu, C.; Yang, B.R.; Xie, X.; Lu, X. Rapid-response, reversible and flexible humidity sensing platform using a hydrophobic and porous substrate. *J. Mater. Chem. B* **2019**, *7*, 2063–2073. [[CrossRef](#)]
27. Shi, J.; Yu, P.; Liu, F.; He, P.; Wang, R.; Qin, L.; Zhou, J.; Sui, X.; Zhang, S.; Zhang, Y.; et al. 3R MoS_2 with broken inversion symmetry: A promising ultrathin nonlinear optical device. *Adv. Mater.* **2017**, *29*, 1701486. [[CrossRef](#)]
28. Chen, Y.; Song, B.; Tang, X.; Lu, L.; Xue, J. Ultrasmall Fe_3O_4 nanoparticle/ MoS_2 nanosheet composites with superior performances for lithium ion batteries. *Small* **2014**, *10*, 1536–1543. [[CrossRef](#)]
29. Chang, K.; Mei, Z.; Wang, T.; Kang, Q.; Ouyang, S.; Ye, J. MoS_2 /graphene cocatalyst for efficient photocatalytic H_2 evolution under visible light irradiation. *ACS Nano* **2014**, *8*, 7078–7087. [[CrossRef](#)]
30. Chen, T.; Yan, W.; Xu, J.; Li, J.; Zhang, G.; Ho, D. Highly sensitive and selective NO_2 sensor based on 3D MoS_2 /rGO composites prepared by a low temperature self-assembly method. *J. Alloys Compd.* **2019**, *793*, 541–551. [[CrossRef](#)]
31. Cho, B.; Yoon, J.; Lim, S.K.; Kim, A.R.; Kim, D.H.; Park, S.G.; Kwon, J.D.; Lee, Y.J.; Lee, K.H.; Lee, B.H.; et al. Chemical sensing of 2D graphene/ MoS_2 heterostructure device. *ACS Appl. Mater. Interfaces* **2015**, *7*, 16775–16780. [[CrossRef](#)] [[PubMed](#)]
32. Li, Q.C.; Chen, D.; Miao, J.; Lin, S.; Yu, Z.; Han, Y.; Yang, Z.; Zhi, X.; Cui, D.X.; An, Z. Ag-Modified 3D Reduced Graphene Oxide Aerogel-Based Sensor with an Embedded Microheater for a Fast Response and High-Sensitive Detection of NO_2 . *ACS Appl. Mater. Interfaces* **2020**, *12*, 25243–25252. [[CrossRef](#)]
33. Long, H.; Harley-Trochimczyk, A.; Pham, T.; Tang, Z.; Shi, T.; Zettl, A.; Carraro, C.; Marcus, A.W.; Maboudian, R. High surface area MoS_2 /graphene hybrid aerogel for ultrasensitive NO_2 detection. *Adv. Funct. Mater.* **2016**, *26*, 5158–5165. [[CrossRef](#)]
34. Zhou, W.; Yin, Z.; Du, Y.; Huang, X.; Zeng, Z.; Fan, Z.; Liu, H.; Wang, J.Y.; Zhang, H. Synthesis of few-layer MoS_2 nanosheet-coated TiO_2 nanobelt heterostructures for enhanced photocatalytic activities. *Small* **2013**, *9*, 140–147. [[CrossRef](#)] [[PubMed](#)]
35. Yin, M.; Wang, Y.; Yu, L.; Wang, H.; Zhu, Y.; Li, C. Ag nanoparticles-modified $\text{Fe}_2\text{O}_3@ \text{MoS}_2$ core-shell micro/nanocomposites for high-performance NO_2 gas detection at low temperature. *J. Alloys Compd.* **2020**, *829*, 154471. [[CrossRef](#)]
36. Donarelli, M.; Bisti, F.; Perrozzi, F.; Ottaviano, L. Tunable sulfur desorption in exfoliated MoS_2 by means of thermal annealing in ultra-high vacuum. *Chem. Phys. Lett.* **2013**, *588*, 198–202. [[CrossRef](#)]
37. Li, J.; Lu, Y.; Ye, Q.; Cinke, M.; Han, J.; Meyyappan, M. Carbon nanotube sensors for gas and organic vapor detection. *Nano Lett.* **2003**, *3*, 929–933. [[CrossRef](#)]
38. Dai, Z.; Lee, C.S.; Tian, Y.; Kim, I.D.; Lee, J.H. Highly reversible switching from P-to N-type NO_2 sensing in a monolayer Fe_2O_3 inverse opal film and the associated P–N transition phase diagram. *J. Mater. Chem. A* **2015**, *3*, 3372–3381. [[CrossRef](#)]
39. Zhang, B.; Liu, G.; Cheng, M.; Gao, Y.; Zhao, L.; Li, S.; Liu, F.M.; Yan, X.; Zhang, T.; Sun, P.; et al. The preparation of reduced graphene oxide-encapsulated $\alpha\text{-Fe}_2\text{O}_3$ hybrid and its outstanding NO_2 gas sensing properties at room temperature. *Sens. Actuators B* **2018**, *261*, 252–263. [[CrossRef](#)]

40. Yao, F.; Duong, D.L.; Lim, S.C.; Yang, S.B.; Hwang, H.R.; Yu, W.J.; Lee, H.; Lee, Y.H. Humidity-assisted selective reactivity between NO₂ and SO₂ gas on carbon nanotubes. *J. Mater. Chem.* **2011**, *21*, 4502–4508. [[CrossRef](#)]
41. Deokar, G.; Vancsó, P.; Arenal, R.; Ravaux, F.; Casanova-Cháfer, J.; Llobet, E.; Anna, M.; Densi, V.; Struzzi, C.; Lambin, P.; et al. MoS₂–carbon nanotube hybrid material growth and gas sensing. *Adv. Mater. Interfaces* **2017**, *4*, 1700801. [[CrossRef](#)]
42. Kim, Y.; Kwon, K.C.; Kang, S.; Kim, C.; Kim, T.H.; Hong, S.P.; Park, S.Y.; Suh, J.M.; Choi, M.J.; Han, S.; et al. Two-dimensional NbS₂ gas sensors for selective and reversible NO₂ detection at room temperature. *ACS Sens.* **2019**, *4*, 2395–2402. [[CrossRef](#)] [[PubMed](#)]
43. Cui, S.; Wen, Z.; Huang, X.; Chang, J.; Chen, J. Stabilizing MoS₂ nanosheets through SnO₂ nanocrystal decoration for high-performance gas sensing in air. *Small* **2015**, *11*, 2305–2313. [[CrossRef](#)] [[PubMed](#)]
44. Zhang, B.; Cheng, M.; Liu, G.; Gao, Y.; Zhao, L.; Li, S.; Wang, Y.P.; Liu, F.M.; Liang, X.S.; Zhang, T.; et al. Room temperature NO₂ gas sensor based on porous Co₃O₄ slices/reduced graphene oxide hybrid. *Sens. Actuators B* **2018**, *263*, 387–399. [[CrossRef](#)]
45. Wu, J.; Wu, Z.; Ding, H.; Wei, Y.; Huang, W.; Yang, X.; Li, Z.Y.; Qiu, L.; Wang, X. Flexible, 3D SnS₂/Reduced graphene oxide heterostructured NO₂ sensor. *Sens. Actuators B* **2020**, *305*, 127445. [[CrossRef](#)]
46. Li, W.; Chen, R.; Qi, W.; Cai, L.; Sun, Y.; Sun, M.; Li, C.; Yang, X.K.; Xiang, L.; Xie, D.; et al. Reduced graphene oxide/mesoporous ZnO NSs hybrid fibers for flexible, stretchable, twisted, and wearable NO₂ E-textile gas sensor. *ACS Sens.* **2019**, *4*, 2809–2818. [[CrossRef](#)]
47. Han, Y.; Huang, D.; Ma, Y.; He, G.; Hu, J.; Zhang, J.; Hu, N.T.; Su, Y.J.; Zhou, Z.H.; Zhang, Y.F.; et al. Design of hetero-nanostructures on MoS₂ nanosheets to boost NO₂ room-temperature sensing. *ACS Appl. Mater. Interfaces* **2018**, *10*, 22640–22649. [[CrossRef](#)]
48. Yang, Z.; Zhang, D.; Chen, H. MOF-derived indium oxide hollow microtubes/MoS₂ nanoparticles for NO₂ gas sensing. *Sens. Actuators B* **2019**, *300*, 127037. [[CrossRef](#)]
49. Kim, D.H.; Jung, J.W.; Choi, S.J.; Jang, J.S.; Koo, W.T.; Kim, I.D. Pt nanoparticles functionalized tungsten oxynitride hybrid chemiresistor: Low-temperature NO₂ sensing. *Sens. Actuators B* **2018**, *273*, 1269–1277. [[CrossRef](#)]
50. Zhou, Y.; Liu, G.; Zhu, X.; Guo, Y. Ultrasensitive NO₂ gas sensing based on rGO/MoS₂ nanocomposite film at low temperature. *Sens. Actuators B* **2017**, *251*, 280–290. [[CrossRef](#)]
51. Mao, S.; Yu, K.; Cui, S.; Bo, Z.; Lu, G.; Chen, J. A new reducing agent to prepare single-layer, high-quality reduced graphene oxide for device applications. *Nanoscale* **2011**, *3*, 2849–2853. [[CrossRef](#)] [[PubMed](#)]